Maintaining and Improving Voltage and Frequency Stability in AC Microgrid Using Adaptive Load Shedding and Battery Storage

Milad Rezaee[1]*, Saeedallah Mortazavi[1] and Alireza Saffarian[1]

Abstract--In recent years, due to economic, technical, and environmental limitations, the expansion of microgrids and their integration with the main distribution network has become an effective solution for optimal use of the power grid. This paper used a hierarchical control strategy in the first and second layers to deal with slight and heavy disturbances that occurred in the islanding mode of operation. The first level is responsible for power sharing using the droop control method, and the second level is tasked with restoring frequency and voltage stability in the case of large disturbances that may lead to collapse and blackout in a microgrid. In this paper, using an energy storage system(battery) and a static synchronous compensator, the stability of important variables of the microgrid is maintained and improved when a small-scale disturbance occurs in the islanding mode of operation. This paper proposes a new adaptive load shedding method with inertia update to maintain frequency stability during large-scale power imbalance. Loads with lower priority are shed, and important variables of the network, i.e., voltage and frequency, are returned to their nominal value. The results show that the control structure in different conditions may maintain the frequency and voltage in the nominal range of the microgrid. The simulations are carried out in MATLAB software.

Index Terms- Energy Storage System, Frequency Stability, Load Shedding, Microgrid.

Nomenclature

Acronyms

AC	alternating current
CHP	combined heat and power
DC	direct current
DER	distributed energy resource
D-STATCOM	distributed static compensator
ESS	energy storage system
MG	microgrid
PCC	point of common coupling
PV	photovoltaic
RoCoF	rate of change of frequency
UFLS	under frequency load shedding
SCADA	supervisory control and data acquisition

Variables

H_i	inertia constant(s)
f	frequency(Hz)
H	inertia equivalent of the total MG
ΔP	power imbalance created in MG(kW)
RoCoF	rate of change of frequency (Hz/s)

I. INTRODUCTION

The rising and consistent demand for electricity globally necessitates an expansion in generation capacity. However, the challenges encountered by generation and marketing service providers have facilitated the emergence and development of distribution generator (DG) technologies. Alongside these DGs, the concept of microgrids has emerged, introducing a range of advantages that were unattainable with traditional radial power systems [1]. The traditional power system is currently confronted with challenges such as the depletion of fossil fuel reserves, inadequate energy efficiency, and environmental degradation [2]. Microgrids are integrated into both alternating current (AC) and direct current (DC) power systems, typically situated close to load centers. This positioning helps to minimize line losses while enhancing reliability and power quality [3]. The correct operation of MG in island mode is specified according to the IEEE1547.4 standards [4]. Numerous researchers have characterized the microgrid's framework as a compact power system that encompasses low-voltage distribution lines, distributed energy resources (DERs) including renewable energy sources like photovoltaic cells and wind turbines, energy storage systems (ESS), microturbines, diesel generators, combined heat and power (CHP) systems, power conversion devices, controllable loads, as well as monitoring and protection mechanisms [5, 6]. The microgrid functions autonomously, demonstrating capabilities for self-regulation and self-administration [7]. Additionally, one of the key benefits of the microgrid is its effective energy management; it ensures the maintenance of energy balance and optimization within the system, delivering high-quality power to users while enhancing the integration of renewable energy sources [8].

The energy storage system is an essential part of the microgrid. Adding a storage system is a smart way to curb power fluctuations and deal with power imbalances [9]. In addition, the storage system plays an important role in improving system reliability and stability in a microgrid, including a large share of renewable resources. Its integration can reduce the cost of improving the transmission and distribution capacity to address the increasing power demand [10]. Therefore, a battery energy storage device is integrated into the microgrid system to deal with the energy shortage.

1. Department of Electrical Engineering, Shahid Chamran University, Ahvaz, Khuzestan, Iran
* Corresponding author:Email: milad.rezaee51@yahoo.com

However, the integration of battery storage devices may not always guarantee a robust transient support system, as these storage elements offer low power density relative to their storage volume. Although these types of storage devices increase the relative inertia of the microgrid, they fail during the transient period. In other words, the microgrid lacks the amount of inertia necessary to resist transient fluctuations caused by system disturbances. Therefore, considerable attention has been drawn to the integration of a distributed static compensator (D-STATCOM) in microgrids.

A key principle is that the microgrid must be capable of functioning in both connected and island modes. Consequently, the microgrid can continue to operate even if an unforeseen disconnection happens between it and the utility at the point of common coupling (PCC) [11, 12]. Nevertheless, microgrids operating in island mode encounter challenges related to voltage and frequency fluctuations, primarily due to the absence of inertia response from distributed energy resources (DERs) [12]. The increasing adoption of distributed energy resources (DERs) is leading to a significant transformation in large-scale power systems, as they gradually replace synchronous generators (SGs) [11]. This shift has resulted in instances of abrupt power generation unit failures or situations where the demand exceeds the available power generation [3]. In the context of microgrids, which can operate in both connected and island modes, the connected mode enables the utility grid to compensate for any power deficits, while excess energy produced by the microgrid can be sold. Conversely, in islanded mode, it is essential to regulate both the frequency and voltage of the system, in addition to supplying the necessary active and reactive power to meet load demands [7].

Typically, the microgrid (MG) is linked to the national grid, facilitating a power exchange between the two. Distributed generators (DGs) are designed to deliver a predetermined amount of power, often aimed at reducing network losses, although this varies across different systems [11]. This arrangement allows the network to serve as a backup, addressing any power imbalances within the MG. Islanding of the microgrid can occur either as a planned event or unexpectedly. During the transition from a grid-connected state to an islanded state, the MG attempts to maintain its previous operational conditions; however, this is often unfeasible. To ensure stability, it becomes necessary to reduce some of the load. When the MG is connected to the main grid, it typically draws power from it. Consequently, in the event of islanding, there will be a power imbalance [11]. To address this issue, a method for ensuring the stability of the isolated microgrid (MG) will be discussed. Similar to conventional systems, disconnected MGs can experience various incidents, including generator failures, imbalances in power consumption, and issues related to power quality. Consequently, effective control mechanisms are essential for the safe operation of MGs. Various local, general, secondary, and emergency control loops are employed to regulate the microgrid [13, 14]. The primary objective of these controllers is to maintain system reliability and facilitate the restoration of normal operations following a disturbance; however, each controller is designed to respond to specific types of disturbances [15]. Minor disturbances typically do not necessitate urgent intervention, whereas significant disturbances require emergency control measures to avert system failure. This article considers load shedding as one of the emergency strategies. Emergency control can be implemented in both supply and demand contexts, with load shedding specifically addressing the demand side. In this approach, certain loads are curtailed to ensure that the available generation capacity can adequately support the remaining loads [16].

Load shedding methods based on intelligent algorithms are implemented according to optimized control schemes, which are accompanied by the modeling of corresponding mathematical equations [17, 18]. In intelligent computational techniques, load shedding is performed optimally; however, the weakness of this load shedding method is the lack of guaranteed compatibility with frequency and voltage instabilities in a combined manner [18]. Load shedding based on intelligent algorithms and computations can be executed through genetic algorithms or neural networks [19].

Various standards and techniques are employed for load shedding. These methods can be classified into two main categories: frequency-based and voltage-based approaches. Among these, frequency load shedding is the most prevalent method, with the rate of frequency fluctuations serving as its primary criterion [15]. Furthermore, during a significant disruption within the system, not only is there a deficiency in active power, but reactive power is also diminished, jeopardizing the stability of voltage and frequency. Consequently, implementing combined load shedding based on frequency and voltage criteria emerges as an effective strategy for managing load shedding. According to the technical conditions affecting the microgrid (MG), it is crucial to consider the following two factors when establishing the criteria for load shedding: – The MG experiences increased frequency fluctuations due to the low and variable inertia associated with the integration of distributed generation sources, such as wind power plants. – The electrical distance between the buses is minimized in the MG, owing to the proximity of generation and load within the low-pressure and medium-pressure systems [20].

Typically, UFLS methods that utilize adaptive and computational intelligence assess the level of disturbance and determine the necessary load shedding based on the degree of imbalance. References [21-27] present adaptive UFLS approaches tailored for traditional power systems. Specifically, in [21], a UFLS strategy is introduced that prioritizes the shedding of loads characterized by a lower VQ margin and suboptimal voltage profiles. In [22], the prediction of frequency trajectories is achieved through the application of the second derivative of frequency, while the quantity of removable loads is assessed via ongoing forecasts of the minimum frequency value. In [23], an index is established for each feeder to identify the specific locations of loads that need to be curtailed. Reference [24] discusses the implementation of Frequency Load Shedding (UFLS) and under-voltage load shedding strategies in a synchronized manner. In [25], predictions regarding

frequency and the time required to reach a specified threshold value are made utilizing a curve fitting approach. A load priority table is employed to identify which loads should be curtailed. Reference [26] discusses the ranking of loads based on the Outage Sensitivity Index (OSI), with load shedding prioritizing those loads that exhibit a higher OSI, indicating a greater potential impact on critical components susceptible to outages. In [27], a three-stage adaptive Underfrequency Load Shedding (UFLS) scheme is introduced, where predetermined loads are disconnected based on the type of event and a lookup table. Reference [28] highlights the use of instantaneous voltage deviations at load buses to establish the threshold for frequency relays; a more significant voltage drop at these buses correlates with elevated frequency thresholds for the relays. Finally, in [29], the frequency threshold values for the relays and the time delays between successive actions are determined based on the voltage reductions observed at the load buses.

The frequency drop rate in microgrids (MGs) is higher than in traditional power systems, primarily due to their lower inertia constant. Consequently, underfrequency load shedding (UFLS) strategies in MGs must operate more swiftly than those in conventional systems. In [30], consumers are prioritized based on their willingness to pay index, and the rate of change of frequency (RoCoF) is assessed for each load. The UFLS process will persist until the cumulative RoCoFs of the loads exceed the overall system RoCoF. In [31], a decentralized under-frequency load shedding (UFLS) strategy is introduced, utilizing the nearest neighboring consensus algorithm (NNCA). This strategy employs a two-tiered approach: the first tier involves estimating the level of disturbance, while the second tier focuses on shedding the identified loads. Likewise, in [32], a two-tiered method is also applied in the implementation of the UFLS scheme. In [33], a gradual process of load shedding is implemented at sites where significant voltage drops and frequency fluctuations occur. Meanwhile, in [34], distributed state estimators are employed to facilitate Underfrequency Load Shedding (UFLS), which systematically reduces the load in four stages based on the magnitude of the disturbance. In [35], a three-stage adaptive under-frequency load shedding method has been employed. In this method, the frequency of the microgrid has been well restored after islanding and being in overload conditions. Additionally, the voltage has remained within the permissible range; however, this method neglects the change in inertia of the microgrid during islanding. In [36], a combined load shedding method of UFLs and UVLs has been used. In this method, the uncertainty in the generation of distributed generation sources and the variability of the microgrid's inertia have not been considered, which leads to suboptimal load shedding.

In this paper, the droop control method is used for DGs in a microgrid to maintain microgrid stability in case of small-scale disturbances by changing the operating point. In the next stages, a multi-level adaptive load shedding method is proposed to deal with large-scale disturbances to prevent microgrid collapse.

II. MICROGRID CONTROL

To achieve a balanced voltage profile and reduce system losses, efficient power sharing is crucial. Power sharing can be controlled by implementing a communication-based centralized control strategy or a decentralized droop strategy. In recent years, communication strategies have been avoided due to economic constraints. Moreover, interruptions and failures in communication are a few limitations for the communication-based control strategy. Hence, decentralized droop control strategies have attracted much attention. Droop control facilitates faster stability and efficient power sharing among distributed generations in a microgrid. The droop strategy can be explained using the main circuit of two AC sources (i.e $V_1 < \delta$ and $V_2 < 0$) connected by an impedance line under reactance (X). Power transfer between two sources may be written as:

$$P = \frac{V_1 \times V_2 \sin \delta}{X} \tag{1}$$

$$Q = \frac{V_1^2 - V_1 V_2 \cos \delta}{X} \tag{2}$$

It can be analyzed that the transmitted active power is proportional to δ, because, during normal operation of the system, the angle tends to decrease. The transmitted reactive power also changes proportionally to the difference between the voltage values at the two ends [37]. Therefore, the droop characteristics may be framed as the following equations which are shown graphically in Fig. 1.

$$\omega = \omega_{max} - m_p P$$

$$m_p = \frac{\omega_{max} - \omega_{min}}{P_{max}} \tag{3}$$

$$V = V_0 - n_q Q$$
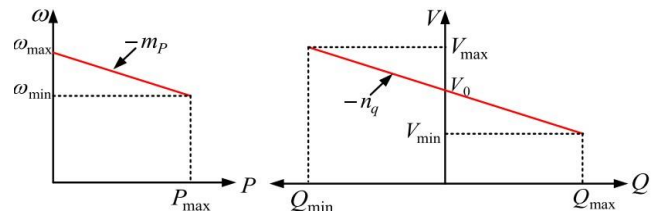
$$n_q = \frac{V_{max} - V_{min}}{2Q_{max}} \tag{4}$$

Fig. 1. Droop characteristics for power-sharing.

Therefore, the control strategy of DGs in a microgrid dominated by inductance implements the characteristics of active power (P-F) frequency drop control and voltage reactive power (Q-V) [38]. With accurate power division between multiple power generators in the microgrid.

III. HIERARCHICAL CONTROL

A microgrid could be operated in both grid-connected and islanded operating modes. Proper microgrid control is a prerequisite for sustainable and economically efficient operation [39]. The main roles of the microgrid control structure are [40, 41]:

- Setting voltage and frequency
- Proper balance of load and production with coordinated distributed energy resources
- Resynchronizing the microgrid with the main grid. Controlling the flow of electricity between the microgrid and the main grid
- Optimizing microgrid operating cost

These requirements have different importance and time scales, so they need a hierarchical control structure to handle each requirement in a different control hierarchy [40]. The hierarchical control strategy consists of three levels, primary controls, secondary controls, and tertiary controls, as shown in Fig. 2. The primary control maintains the voltage and frequency stability of the microgrid after the islanding process. It is necessary to provide independent active and reactive power sharing controls for DERs in the presence of linear and nonlinear loads. In addition, power-sharing control prevents unwanted currents from circulating. This primary control level includes the basic control hardware, which is usually called the zero level. This level includes the internal voltage and current control loops of DERs.
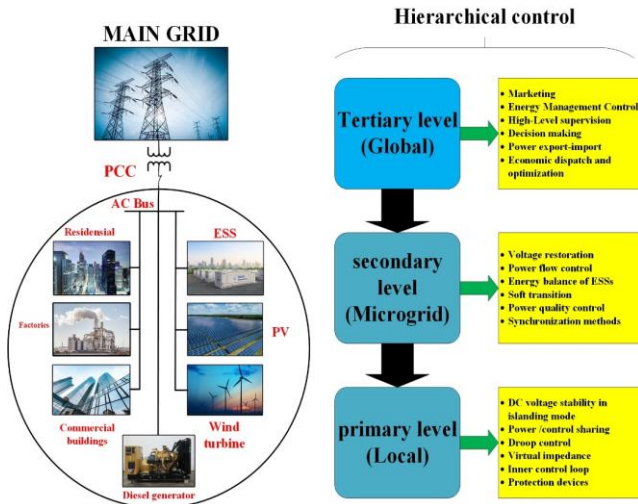

Fig. 2. Principle of microgrid Hierarchical control.

The secondary control compensates for the voltage and frequency deviations caused by the operation of the primary controls. Finally, at the tertiary level, when the microgrid is operating in grid-connected mode, the power flow can be controlled by adjusting the frequency (changing the phase in a steady state) and amplitude of voltage inside the microgrid. In this paper, the use of a decentralized and local control structure is proposed in the primary and secondary levels to control frequency and voltage.

IV. LOAD SHEDDING

Advanced methods in load shedding, known as adaptive techniques, normally use the frequency derivative and depend on the frequency response of the system (SFR2) [42]. Bo Y, et al. show that by using real-time system frequency changes, the adaptive method can be generally accurate in determining the load that should be shed [43]. Adaptive load shedding curtails a more accurate amount of loads when the microgrid is faced with a power imbalance. Determining the amount of power deficit is the first stage in load shedding schemes. Adaptive load shedding usually uses a swing equation to shed the required amount of load. Power deficit can be computed using the following equation [44]:

$$\Delta P = \frac{2 \times H}{f_n} \times \frac{df}{dt} \tag{5}$$

In this regard, ΔP is the power imbalance value, H is the inertia constant of the generator, f is the nominal frequency (Hz), and df/dt is the rate of change of frequency (Hz/s). The parameters required to implement an adaptive scheme are readily available in the central control and may be transmitted to the relays through the SCADA system. Huang et al. believed that this adaptive load shedding technique is robust and insensitive to transient SCADA failures [45]. Despite an efficient power-sharing strategy, the microgrid may become unstable while experiencing overload conditions. In independent mode, distributed energy resources sacrifice their frequency and voltage to increase power generation. This results in a drop in voltage and frequency that may exceed the specified threshold and cause the system to shut down. A self-governing microgrid addresses the power shortage either by increasing power generation or by reducing power demand. As a result, the system response due to an increase in generation or a decrease in load demand is incorporated to restore voltage and frequency stability.

This paper proposes a load shedding strategy along with power sharing.

An adaptive load-shedding strategy based on inertia updating is used in this paper, which deals with the power imbalance in the microgrid after an islanding event. The rate of change of frequency is considered to calculate the amount of load to be shed. At the beginning of the load shedding algorithm, it confirms the existence of a storage system. The stored battery power supports the load for a certain period. The first stage of the strategy controls the rapid frequency drop by shedding large loads. It causes the system frequency to be placed at the specified low operating limit (F≥59.3 Hz). Therefore, the frequency threshold is set to be 59.3 Hz, and the time delay for the UFLS is 0.2 s [46, 47]. Since the microgrid has minimal inertial stability, it becomes very sensitive to the dynamic load demand. This sensitivity increases the instability of the system by increasing the frequency deviation. Therefore, in the second and third stages of the proposed load shedding algorithm, it has been observed that the working frequency tends to maintain the nominal frequency (60 Hz). To reach the predetermined operating value of the system frequency, the

second step of the load shedding strategy starts and reduces small loads in iterative steps. According to [48], for an islanded MG, RoCoF is calculated by applying intentional disturbances. Subsequently, the third stage of load shedding reduces the difference between the operating frequency and the nominal frequency to almost zero by removing very small loads. The frequency deviation in this paper is considered to be 0.05 Hz [49]. A flowchart of the proposed load shedding scheme is presented in Fig. 3, and each shedding step is examined in the next section.
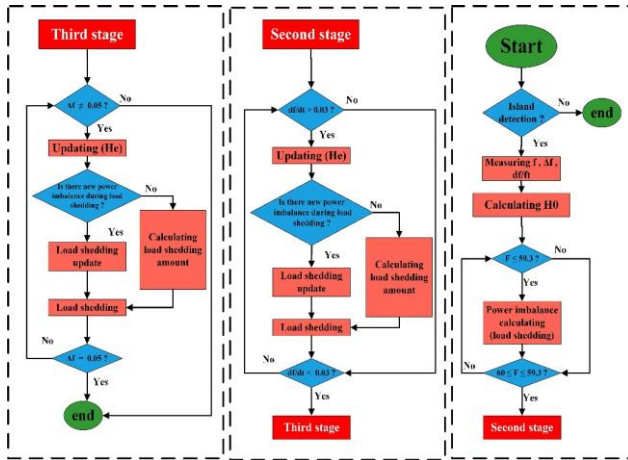
Fig. 3. Flowchart of the proposed load shedding method.

As shown in Fig. 3, the proposed method begins with the islanding of the microgrid. Initially, the frequency, frequency deviation, and its rate of change are measured for the necessary calculations. Subsequently, the initial inertia of the microgrid is calculated using Equation Ⅴ. In the next phase, since the goal is to restore frequency under heavy overload conditions, the frequency threshold is considered to be 59.3 Hz; therefore, for lower frequencies, load shedding is performed. Then, using Formula 5, the amount of power imbalance is specified, and load shedding is performed accordingly. If, after load shedding, the frequency falls within the permissible range, load shedding proceeds to the second stage, where the rate of frequency change is calculated. At this stage, due to changes in the inertia of the microgrid, it needs to be updated, so the inertia is updated using Equation 8. If a new disturbance occurs in the next stage, it is necessary to update the inertia again and perform load shedding accordingly (equation 9) to prevent the disconnection of excess load. If there is no new disturbance, load shedding is carried out with the previous update. Then, it enters the final stage, and to restore the frequency to the nominal range, the inertia is updated again. In this phase, the occurrence of a new disturbance is also examined, and if a new disturbance is present, the inertia is updated once more, and load shedding is performed according to the new value. Finally, the frequency returns to the nominal range.

Due to the presence of distributed generation that is affected by environmental conditions, the inertia of the microgrid is not constant. Considering the equivalent inertia of the microgrid as a constant leads to incorrect and unrealistic calculations and analyses. Hence, it is necessary to estimate it accurately by the dynamic and momentary state of the microgrid. Therefore, it sought to obtain the inertia constant of the microgrid variably and momentarily. On the other hand, distributed energy resources such as photovoltaic and wind, which are affected by weather conditions, have variable production, adding uncertainty to other network constraints. This will complicate the control, protection, and operation of the microgrid. The equivalent inertia(H) and uncertainty in DGs(photovoltaic) have been considered for the load shedding scheme proposed in this paper.

A very important point in load shedding and maintaining the stability of power systems is the accurate estimation of the amount of power shortage through the fluctuation equation. To obtain the exact amount of load shedding, it is necessary to calculate the inertia constant of the system. The microgrid consists of inverter-based distributed generation in addition to synchronous generators. Therefore, the estimation of the equivalent inertia constant of the microgrid must be done online during the load shedding process. In this paper, an attempt is made to calculate the exact amount of power imbalance using a step-by-step calculation. Online estimation of the constant value of microgrid inertia equivalent in each stage of adaptive load shedding will prevent the disconnection of additional loads. This strategy involves the operation of a battery storage system and a distributed D-STATCOM static compensator in the microgrid. This strategy provides customers with a reliable power supply for significant periods instead of sudden load shedding. The rate of change of frequency changes significantly during the transition between stages. The load shed during one iteration is calculated using:

$$P_{LOADSHEDDING} = K \times abs(\frac{df}{dt})$$

$$K = \frac{2 \times H_{equivalent}}{f_{rated}} \qquad (6)$$

Where, $P_{LOADSHEDDING}$ is the amount of load shed in each iteration and K is the shedding constant obtained from the swing equation of the system. $H_{equivalent}$ is the normalized inertial constant. In this formula, (H) represents the normalized inertia constant, which is estimated online at each stage of load shedding. The amount of imbalance in the system is calculated through equation (6), and according to the new value, load shedding will be done in each step. The inertia constant of the microgrid may be calculated based on the rated power of the system. The inertia constant is determined after distributed generation is working in the MG through the following relationship:

$$H_{equivalent} = \frac{\sum_{i=1}^{n} H_i \times S_i}{\sum_{i=1}^{n} S_i} \qquad (7)$$

Using the formula (7), it is possible to estimate the equivalent inertia of the microgrid and calculate the amount of power shortage by placing it in the fluctuation equation. Then apply the load shedding process according to the flow chart (Fig. 3) based on the amount of power imbalance. In islanded microgrids, due to the presence of inverter-based distributed generation, along with synchronous generators, the equivalent inertia is variable with time. Due to the uncertainty and dependence on weather conditions, the production power of inverter-based resources is variable with time. Therefore, to accurately calculate the power imbalance in the microgrid, the swing equation must be used. It is necessary to update and calculate the equivalent inertia value of the microgrid for load shedding from the second stage onwards. The following formula is used to update the equivalent inertia value of the microgrid [50]:

$$H_e(i) = \frac{f_N \times P_{sh_{i-1}}}{2 \times (f'_{a_{i-1}} - f'_{b_{i-1}})} \tag{8}$$

Where, f_N represents the nominal value of the frequency. $P_{sh_{i-1}}$ represents the power of the load interrupted in the stage(i-1), $f'_{a_{i-1}}$ and $f'_{b_{i-1}}$ are the derivatives of the frequency before and after the load shedding stage (i-1), respectively. From the above equation, the equivalent inertia value of the microgrid is updated in each stage of load shedding by placing it in the swing equation. The amount of power deficiency will be calculated in the next stages.

It can be seen from Fig. 4 that the frequency change rate in PCC is significantly high and is a direct factor related to the power deficit. In the occurrence of an island, a significant difference in the rate of change of frequency occurs due to the reduction of the moment of inertia of the microgrid forming the grid. As a result, the amount of load shedding is directly proportional to the frequency derivative. In addition, Fig. 4 shows that with each step of load shedding, the rate of change of frequency decreases with the reduction of the power shortage and tends to almost zero. Therefore, by fulfilling equation (6), it can be analyzed that the amount of load shedding reduces with the reduction of the rate of frequency change (rocof). Therefore, this load shedding strategy presented in Fig. 4 helps to reduce the proportional amount of load shedding related to power shortage.
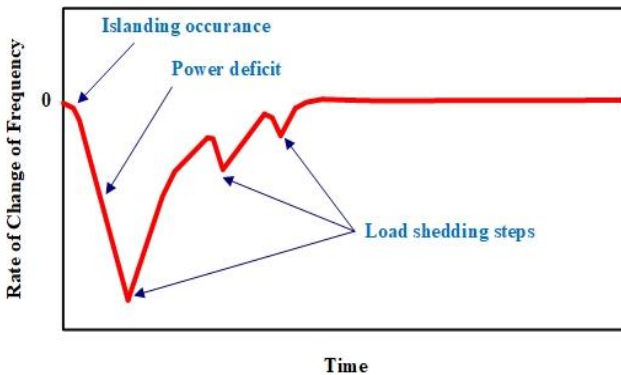

Fig. 4. RoCoF. Considering the lack of power.

In microgrids, the output power of some generating units, such as wind turbines or solar cells, may change suddenly during the load shedding process. Therefore, it is necessary to continuously update $P_{LOADSHEDDING}$ during the load shedding process. A sudden decrease in $P_{LOADSHEDDING}$ caused by a decrease in load or an increase in the output power of generating units may lead to an incremental change in the frequency derivative. On the other hand, the sudden increase in $P_{LOADSHEDDING}$ caused by the sudden decrease in the output power of the generating units leads to a decrease in the frequency derivative step by step. Consequently, when additional power deficits occur during the load-shedding process, Pd($P_{LOADSHEDDING}$) can be updated for subsequent load-shedding steps using (9).

$$P(d_{new}) = P(d_{old}) + \frac{2 \times H_{equivalent}}{f_N} \times \Delta f'(t = t_{ch}) \tag{9}$$

where, $P_{d_{new}}$ and $P_{d_{old}}$ represent the power imbalance in the new and previous stages, respectively. t_{ch} represents the moment of occurrence of an additional power shortage in the system, and Δf is the change in the frequency derivative. The load shedding process continues until the frequency converges to the allowed range and tends to its nominal value in the next steps.

V. SIMULATION AND RESULTS

In this section, to evaluate the Robustness analysis state in the target microgrid, Simulink 2018 software has been used to simulate the proposed approach. As shown in Fig. 5, the studied microgrid is a modified IEEE 13-buses test. Fig. 6 also shows the microgrid simulation in MATLAB Simulink. The system parameters are presented in the Appendix. The size of loads and the location of each load are presented in Table I, and line data are given in Table II.

TABLE I
The Location and Amount of Loads

Load number	Bus number	Load(kW)	Load (kVAR)	Priority
1	5	13.2	1.3	Non-vital
2	8	49	7.7	vital
3	7	10	0.5	Non-vital
4	4	12.8	1.28	vital
5	7	5.5	0.45	Non-vital
6	13	20.5	5.75	vital
7	9	2.3	0.23	Non-vital
8	11	4.7	0.47	Non-vital
9	10	15	7.5	vital
10	6	7.5	0.75	Non-vital
11	1	17.2	0.5	Non-vital
12	3	5.5	0.5	Non-vital
13	12	7	0.5	Non-vital
14	6	4.2	0.5	Non-vital
15	2	2.4	1.5	Non-vital
16	9	6.4	0.5	Non-vital

TABLE II
Line Data of MG

From	to	R(Ω)	X(Ω)
1	2	0.2	0.0183
1	7	0.1	0.0183
7	8	0.01	0.0183
2	5	0.2	0.0183
5	6	0.2	0.0183
2	3	0.3	0.036
3	4	0.1	0.0183
3	9	0.1	0.0183
9	10	0.1	0.0183
3	11	0.2	0.0183
11	12	0.2	0.0183
12	13	0.2	0.0183
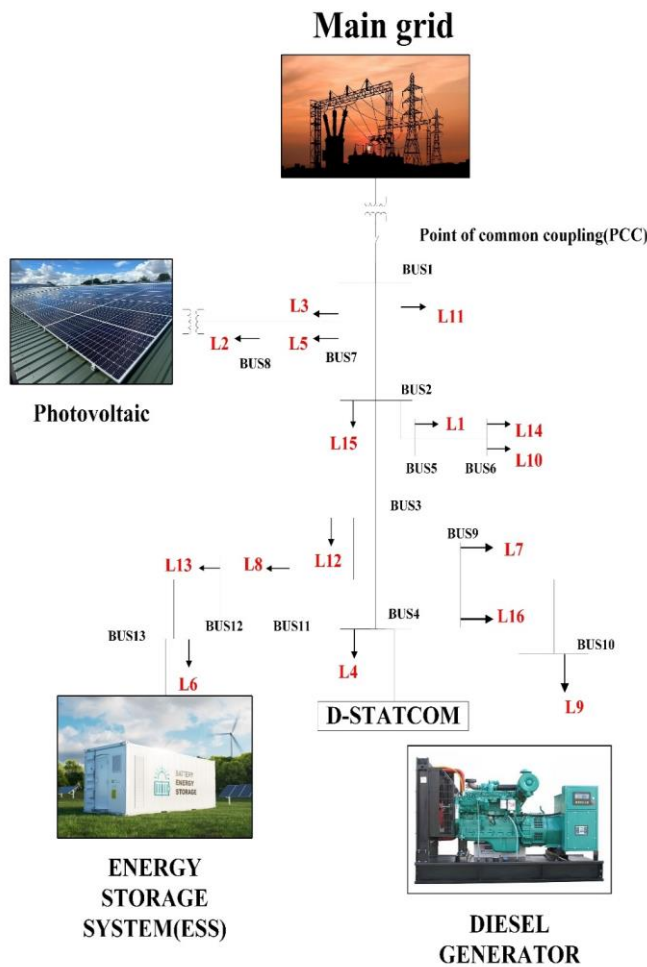
Fig. 5. 13-bus microgrid under study.

At first, the microgrid is connected to the main grid. At a certain moment, through the circuit breaker at the PCC, it will go into an island mode, and fluctuations will occur in the variables. In this microgrid, a diesel generator with a rated power of 50 KVA is used to feed active and reactive power simultaneously, and a solar array with a capacity of 100 kW is used to feed active power. A lithium battery and a static synchronous compensator have been installed to improve the

transient stability of the microgrid and reduce stress on the diesel generator. In the next part, different scenarios for the simulation study are explained. Various scenarios have been considered to validate the proposed load shedding scheme.
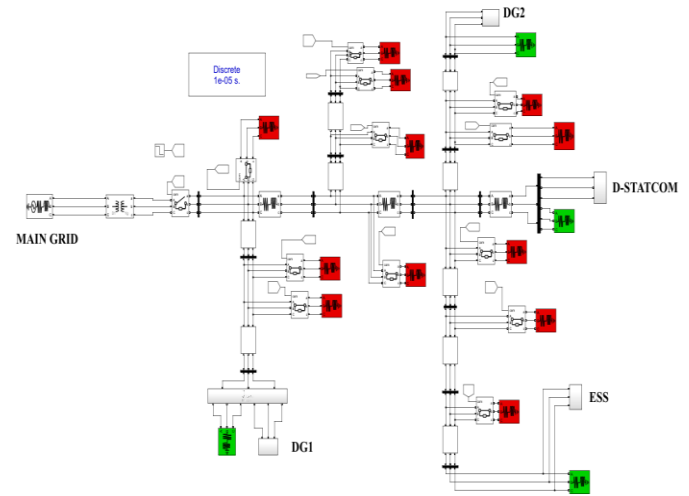

Fig. 6. Simulation model of microgrid using MATLAB/Simulink.

A. Scenario 1

The first scenario is to evaluate the power sharing in the microgrid in the presence of energy storage. At first, the microgrid is connected to the main grid, and then at t=1s, the microgrid goes into an island mode through the circuit breaker of the PCC point. Due to the presence of a 10% overload, the frequency of the microgrid drops.

Before the islanding state, some of the microgrid loads and the task of charging the battery were the responsibility of the main grid. Microgrid islanding, shortage of power causes the basic variables of the microgrid (including voltage and frequency), suffer to fall. This scenario is considered without the presence of a static synchronous compensator. On the other hand, since the solar array is operating in the state of MPPT, the task of supplying additional power is the responsibility of the diesel generator. This causes the frequency of the diesel generator to drop. Therefore, in this case, the existence of the battery as an energy storage device plays an important role. Discharging storage at the isolating moment reduces the stress on the diesel generator and leads to maintaining the frequency and voltage within the permissible range.

As can be seen in Fig. 7a, the battery is in charging before islanding (connected to the upstream network) and immediately releases its rated power due to its rapid dynamics after islanding. It is shown in Fig. 7b that it immediately starts discharging at the islanding moment. Hence, the diesel generator, along with the battery, gets the ability to control the microgrid variables in the presence of 10% overload. According to the controller designed for the battery, the battery is discharged in two stages. First, it discharges its maximum power at the islanding moment (t=1s). Then at t=2.45s, when the SOC value of the battery reaches 50%, the battery power is halved. At t=3.63s when the battery attains 30% of SOC, the power fed by the battery is approximately zero. The active power fed by a battery based on SOC is illustrated in Fig. 7b.
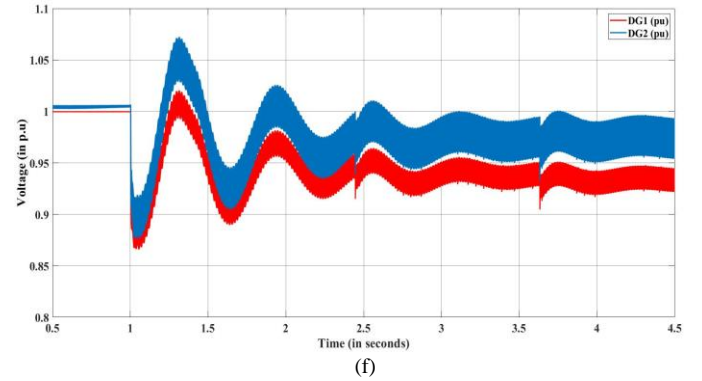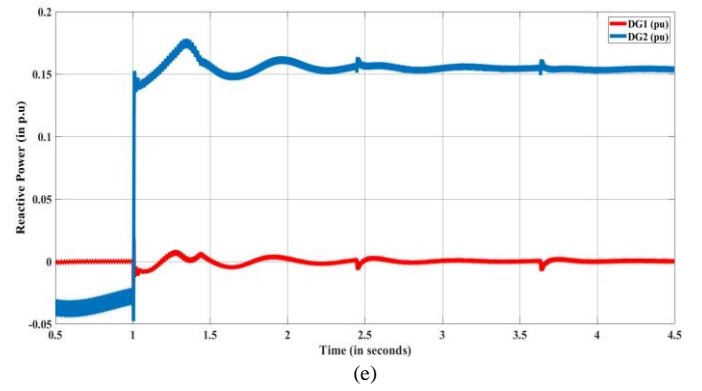
(a)

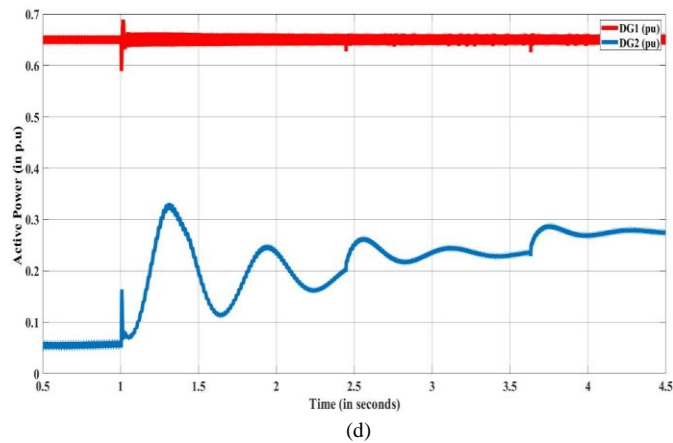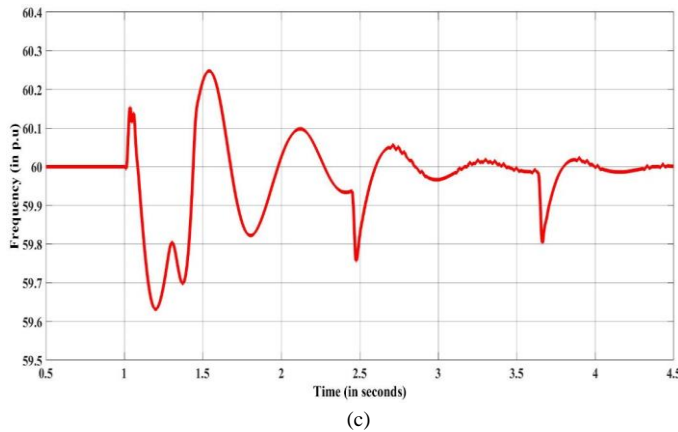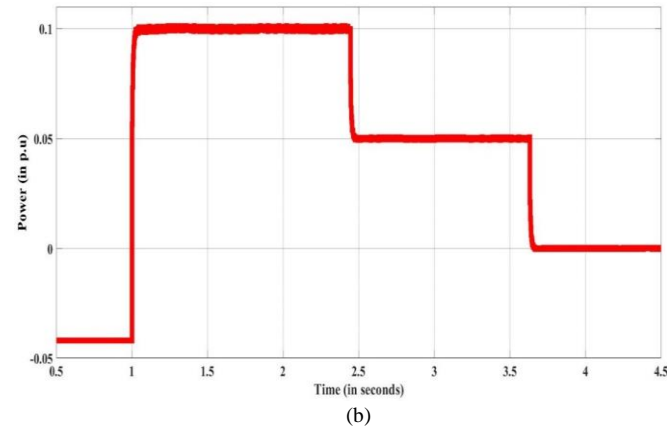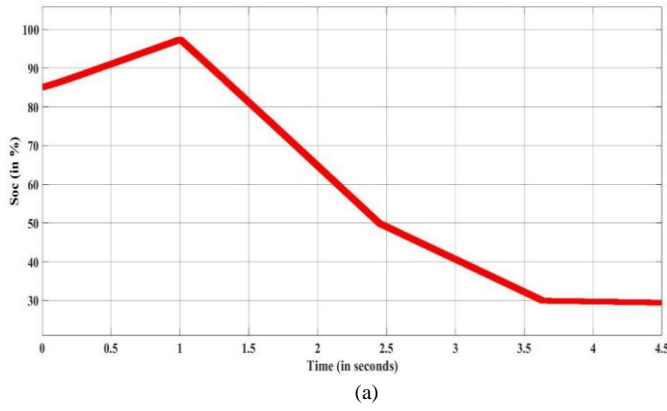
(b)

(c)

(d)

(e)

(f)

Fig. 7. Battery SoC, (b) battery power, (c) frequency, (d) Active power of DG1 and DG2, (e) Reactive power of DG1 and DG2, (f) Voltage of DG1 and DG2

In Fig. 7c and Fig. 7d, the frequency of the microgrid and the active power of distributed energy resources can be observed and checked, respectively. At the islanding moment, due to the loss of the main grid and the existence of a 10% overload, the frequency of the microgrid has dropped. The diesel generator is trying to compensate for this lack of power. Moreover, in the moments of battery discharge in the second and third stages, it can be seen from the above Fig. of part 7d that the diesel generator compensates for the reduced power of the battery. As illustrated in Fig. 7c, diesel generator compensation has led to fluctuations in the frequency of the microgrid, but the frequency reaches its rated value again. Fluctuations in reactive power and voltage are shown in Fig. 6e and Fig. 7f. Due to the use of a photovoltaic source in unit power factor mode, it is not able to exchange reactive power, and only active power exchange is possible. Therefore, the feed of reactive power has been done only by the diesel generator.

B. Scenario 2

The second scenario of this paper is an extension of the first scenario. In the first scenario, the compensation of active power of the loads fed through the main grid, along with the overload, was the responsibility of the diesel generator and the battery. However, the compensation of the reactive power in the microgrid was only through the diesel generator. In the second scenario, using static synchronous compensator (D-STATCOM) is used to improve the stability during transient and after islanding in the microgrid. The aim is to reduce fluctuations in the basic variables of the microgrid. However, to compensate for the reactive power, especially at the moment of islanding in the microgrid, D-STATCOM is connected. It starts producing reactive power required by the microgrid along with

the diesel generator. The simulation results of the second scenario of the microgrid in the presence of D-STATCOM are presented in Fig. 8.

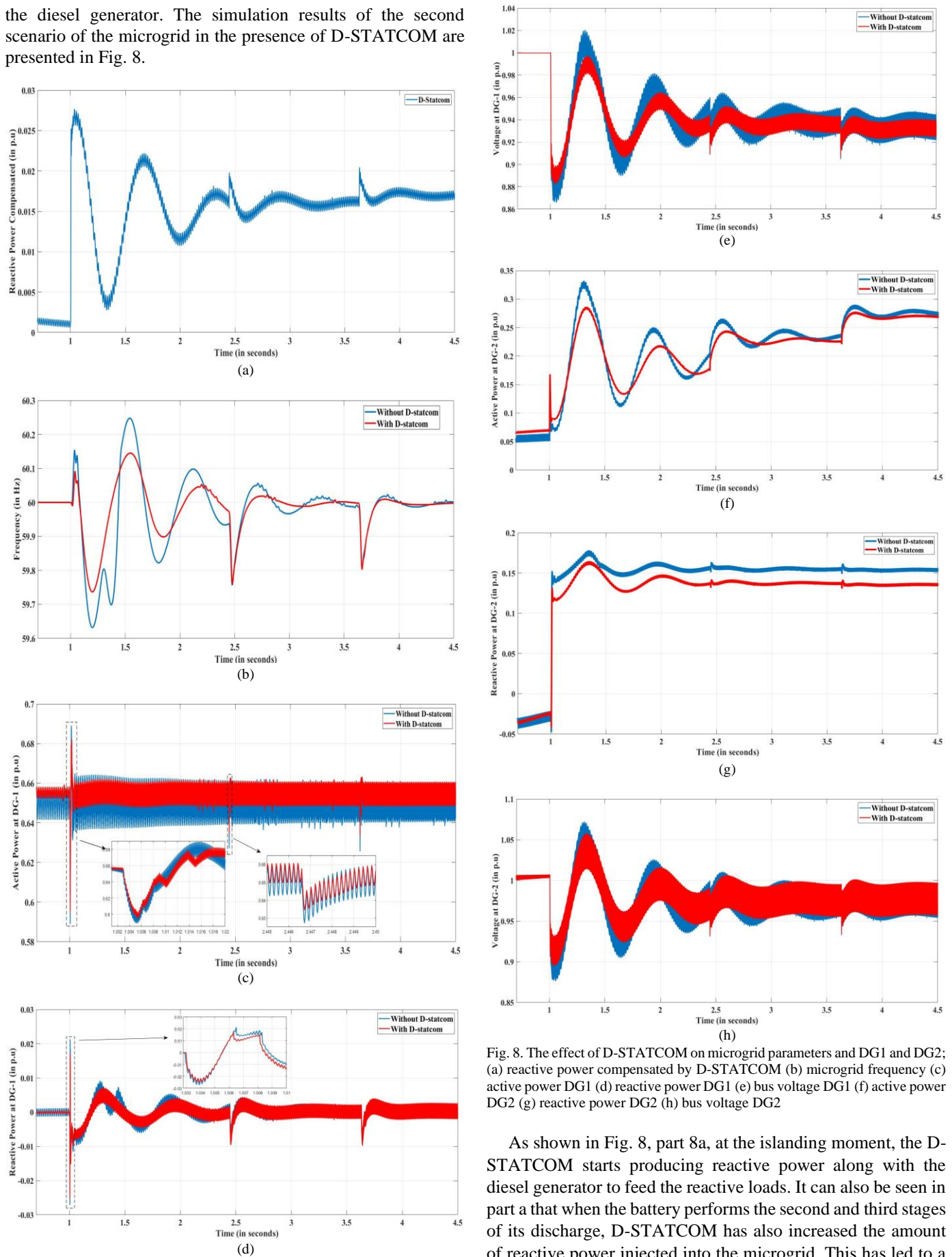
(a)

(b)

(c)

(d)

(e)

(f)

(g)

(h)

Fig. 8. The effect of D-STATCOM on microgrid parameters and DG1 and DG2; (a) reactive power compensated by D-STATCOM (b) microgrid frequency (c) active power DG1 (d) reactive power DG1 (e) bus voltage DG1 (f) active power DG2 (g) reactive power DG2 (h) bus voltage DG2

As shown in Fig. 8, part 8a, at the islanding moment, the D-STATCOM starts producing reactive power along with the diesel generator to feed the reactive loads. It can also be seen in part a that when the battery performs the second and third stages of its discharge, D-STATCOM has also increased the amount of reactive power injected into the microgrid. This has led to a

decrease in the range of fluctuations in the parameters of the microgrid. The presence of D-STATCOM in the circuit has reduced the stress on the diesel generator to produce reactive power. This prevents violation of the production limits for the diesel generator. As illustrated in Fig. 8, with the presence of D-STATCOM, the transient stability has increased, and the range of fluctuations in the frequency and voltage of the microgrid has decreased.

C. Scenario 3

In this scenario, the desired islanded microgrid includes 30% active overload and 10% reactive overload. At t=1s, the islanding of the microgrid and the disconnection of the main grid lead to a drop in frequency and voltage, which is shown in Fig. 9. After the islanding, the local controllers try to compensate for the power imbalance caused by the DGs in the microgrid. However, it fails to control the frequency after a short period and violates the frequency of the allowed frequency range. At the same time of islanding, the battery located in bus 13 starts to discharge with the value of 0.1 p.u. and completely discharges at two break points in the SOC diagram. Fig. 10a and Fig. 10b show the generated active power and battery SOC, respectively.
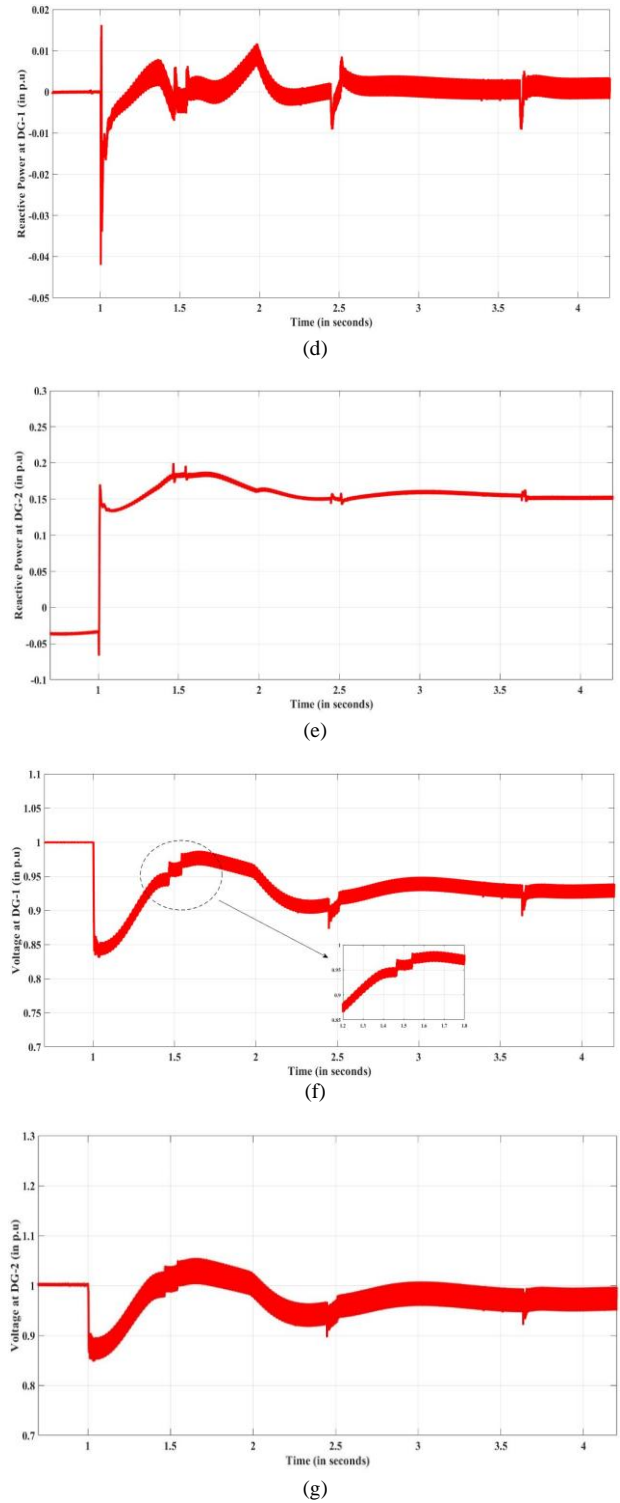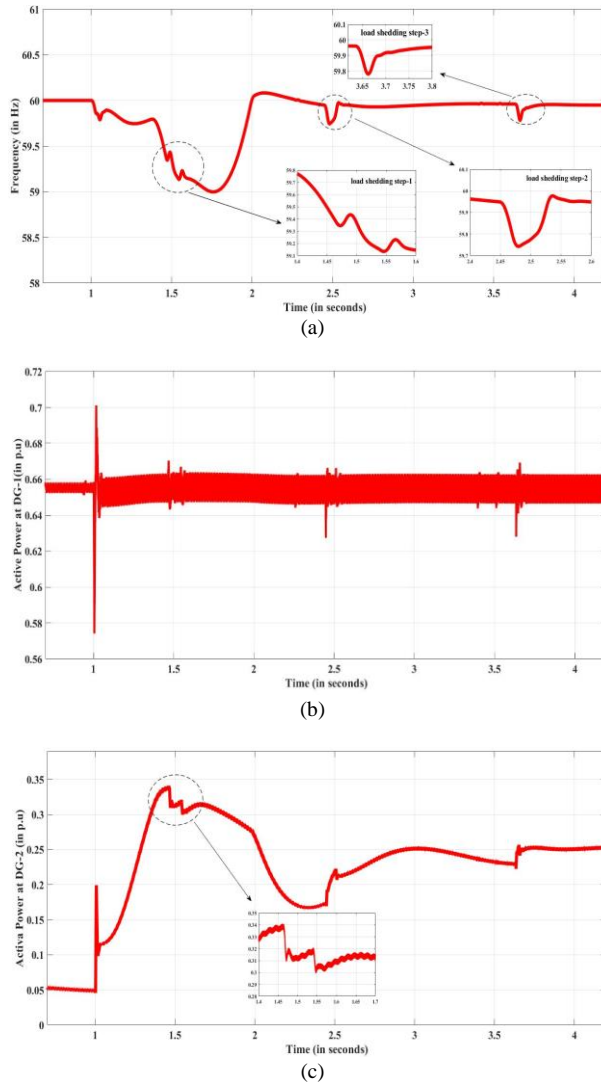

(a)

(b)

(c)

(d)

(e)

(f)

(g)

Fig. 9. The effect of load shedding on microgrid parameters and DG1 and DG2; (a) microgrid frequency, (b) active power DG1, (c) active power DG2, (d) reactive power DG1, (e) reactive power DG2, (f) bus8 voltage, (g) bus10 voltage.

In this scenario, using the updated equivalent inertia of the microgrid is performed in each stage of load shedding. Thereby, updating the instantaneous power imbalance in the microgrid, the values are different from the previous stages. Hence, the load shedding by this method is optimal, and less load will be shed from the microgrid.

As illustrated in Fig. 9, at the islanding moment and frequency drop, the local controllers try to control the power imbalance, but it fail. And at 1.38 seconds, it starts to drop sharply and moves towards collapse. However, at 1.46 and 1.55 seconds, loads were shed twice by sending a disconnection signal from the relay to the corresponding circuit breakers. Thereafter, the microgrid gets the ability to restore the frequency.

Then, at 2.45 sec, the battery in the microgrid goes through the second stage of discharge. Once again, there is a fluctuation in frequency. The frequency of the microgrid drops again, and the diesel generator must increase its production power to compensate for the power imbalance. At this moment, even though the frequency remains within the permissible range, to return it to the nominal value, the load shedding algorithm sends the interrupt command again. Fluctuation in active power produced by DG1 and DG2 is shown in Fig. 9b and Fig. 9c. As can be seen since the solar array is in MPPT mode, it is not able to increase production, and the diesel generator and battery are responsible for active overload control.
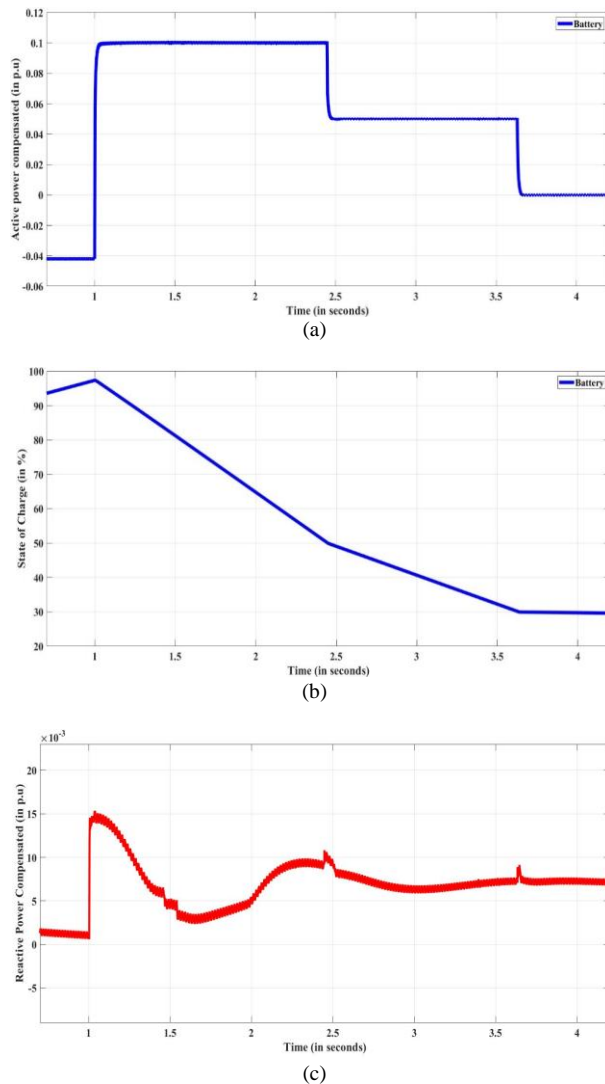

(a)

(b)

(c)

Fig. 10. Power compensated by the storage system and D-STATCOM; (a) active power compensated by battery. (b) battery SoC. (c) Reactive power compensated by D-STATCOM.

Moreover, to participate in reactive power control and reduce the stress on the diesel generator, the amount of power produced by D-STATCOM is shown in Fig. 10c. Clearly, the synchronous compensator controller starts to produce reactive power at the islanding moment. At the islanding moment, D-STATCOM starts producing power at every stage of load shedding. During interruption of loads which includes both active and reactive powers (based on necessity), the reactive power produced by D-STATCOM gets reduced also.

D. Scenario 4

In this scenario, one of the inherent characteristics of distributed generation resources, i.e., uncertainty in power generation, is included. In this way, it is assumed that at a certain moment, the microgrid has gone into an island state. In the beginning, the amount of power produced by the sources is equal to the amount of load. Then at t=2s, the power of the DG1 due to the decrease in sunlight from 1000w/m2 to 800w/m2 has decreased from 90 kW to 80 kW (equivalent to 0.66 and 0.55 p.u), respectively. This leads to a power imbalance in the Microgrid. According to the local microgrid controllers, the diesel generator immediately starts to compensate for the lost power and covers this amount by increasing the level of active power production at the solar array power reduction. The load-shedding algorithm for this case of simulation is designed in such a way that as soon as the production power of the solar array drops, the algorithm starts load shedding in case of emergency.
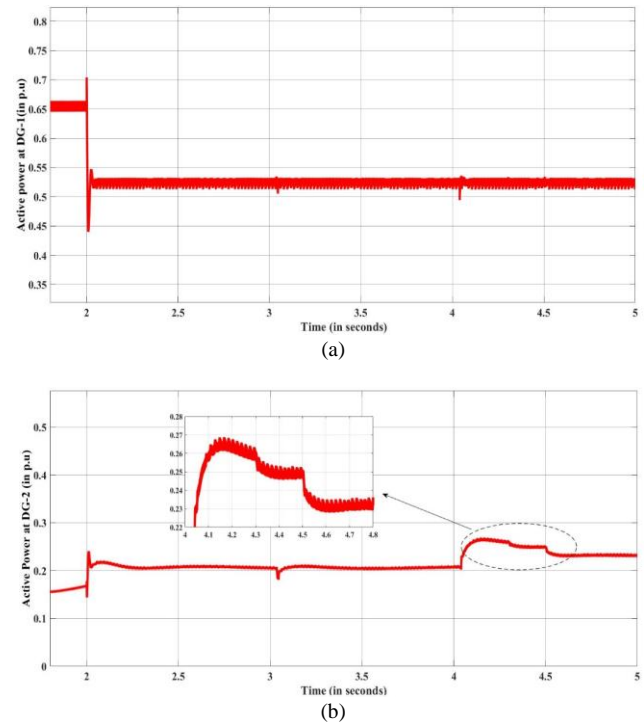

(a)

(b)

Fig. 11. (a) Power generation reduction of DG1. (b) Power generation of DG2

In this scenario, the equivalent inertia value of the microgrid is updated in each step. Then the amount of power deficit in the microgrid is updated. Accordingly, the proposed algorithm uses optimal load shedding according to the current conditions in the microgrid. Fig. 11a shows the photovoltaic

power reduction. The production power of the diesel generator is illustrated in Fig. 11b.
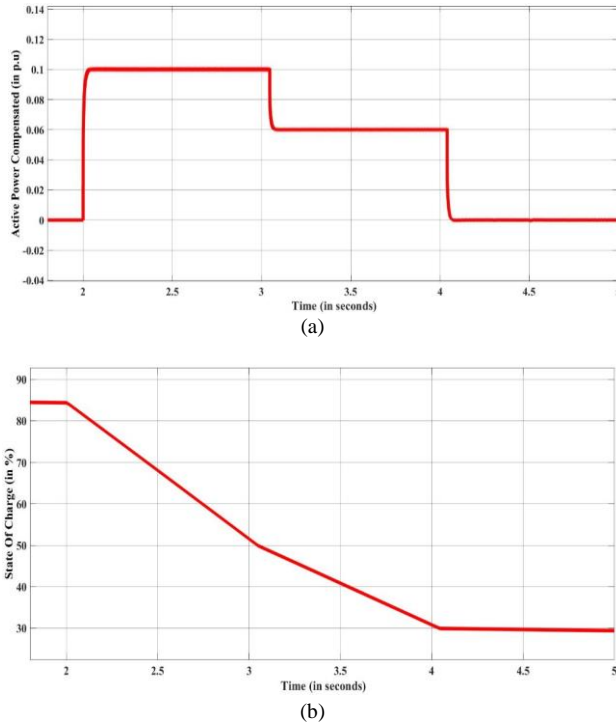

(a)

(b)

Fig. 12. Energy storage parameters: (a) active power, (b) charging mode.

As illustrated in Fig. 11, at t=2s when the power generated by the photovoltaic reduces, the diesel generator immediately starts compensation. The imbalance of power is compensated with the help of the energy storage device shown in Fig. 12.

As shown in Fig. 12, to reduce the stress of the diesel generator, along with the detection of power loss in photovoltaics, the battery has compensated for 0.1 per unit (equivalent to 15 kW) of the power shortage in the microgrid. Also, in Fig. 13, the microgrid frequency is shown during the above steps. As shown in Fig. 13, islanding occurred at 0.5 seconds, after which the frequency was restored.
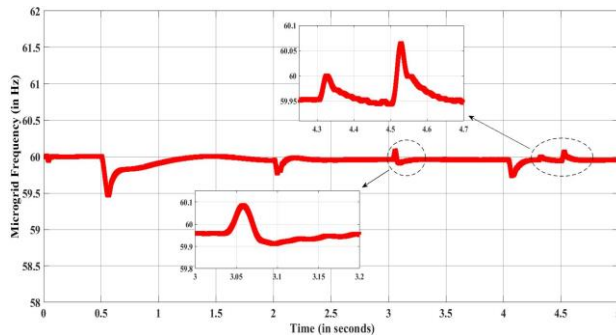

Fig. 13. Microgrid frequency

At 2 seconds, due to the reduction in the production power of the solar array, the frequency fluctuated. With the presence of the diesel generator and energy storage, this deficiency has been compensated, and the frequency is kept within the allowed range. To return the frequency to the nominal range($\Delta f < 0.05$). Fig. 14 shows the frequency deviation from the nominal value (60 Hz).
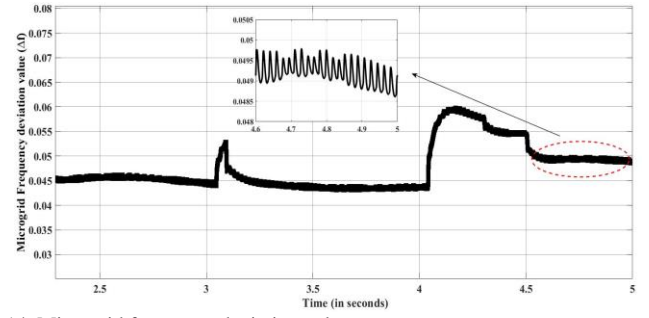

Fig. 14. Microgrid frequency deviation value.

As shown in Fig. 14, to return the microgrid to less than 0.05 Hz difference with the nominal value, two stages of the proposed adaptive load shedding have been used (stages 2 and 3). This resulted in load shedding at the moments of 3.05 seconds(stage 2), and two small load sheds at 4.28 seconds and 4.5 seconds(stage 3), respectively. Finally, the frequency difference from the nominal value has reached less than 0.05 Hz, and the algorithm has successfully brought the frequency to the nominal range.

In Table III, a comparative study of the proposed strategy with the state of the art has been presented.

TABLE III
Comparative Study of the Proposed Load Shedding Strategy With the State of the Art

Ref	RERs impact	Optimal load shedding control	Adaptive strategy for UFLS
[51]	✓	✗	✗
[52]	✗	✗	✓
[53]	✓	✗	✗
[54]	✓	✗	✗
[55]	✗	✓	✗
[56]	✓	✗	✗
[57]	✗	✗	✓
[58]	✗	✓	✓
[59]	✗	✓	✗
[35]	✓	✗	✓
[36]	✗	✗	✓
This paper	✓	✓	✓

VI. CONCLUSION

In this paper, droop control is used for accurate power sharing among the distributed energy resources in a microgrid. Distributed energy resources such as diesel generators, solar arrays and energy storage, and D-STATCOM are used to compensate for small and large-scale disturbances. Tries to improve the transient stability at the moment of islanding and after the islanding of the microgrid. Moreover, in case of large-scale disturbances, a proposed adaptive load shedding method has been used to ensure the control of the microgrid in different

conditions. The simulation study is done in MATLAB. Results in the first scenario show that the presence of the battery (due to its timely presence in the role of an active power generator) has kept the frequency of the microgrid within the permissible range and reduced the stress on the diesel generator. Hence, it helps to control the frequency of the microgrid. In the second scenario, the results indicated the improvement of transit stability using the D-DSTATCOM. It reduces the range of fluctuations of the variables of distributed energy resources by compensating reactive power during islanding and after that. Results of more scenarios under heavy overload show that the microgrid can maintain and improve its stability with the proposed adaptive load shedding scheme.

VII. APPENDIX

Nominal frequency	60Hz
Nominal voltage	25kV
Base power	150 kVA
DG1(PV)	100kW
DG2 (diesel generator)	50Kva(p.f=0.86)
Number of poles(DG2)	4
Number of phases (DG2)	3
Speed (DG2)	1500 rpm
mp	5e-5 Hz/W
nq	0.1667V/Var
T1	115kV/25kV
T2	260V/25kV
ESS:	
Battery rating (Q)	0.226Ah
Rated $V_{battery}$	300 V
E0	305V
Rated $I_{battery}$	120 A
R_{int}	40mΩ
$T_{battery}$	300V/25kV
D-STATCOM:	
DC capacitance	520μF
Maximum compensation	10kVAR
Series reactance	4.8μH

REFERENCES

[1] K. Twaisan and N. Barışçı, "Integrated distributed energy resources (DER) and microgrids: Modeling and optimization of DERs," *Electronics,* vol. 11, no. 18, p. 2816, 2022.

[2] M. Mohebbi-Gharavanlou, S. Nojavan, and K. Zareh, "Energy management of virtual power plant to participate in the electricity market using robust optimization," *Journal of Operation and Automation in Power Engineering,* vol. 8, no. 1, pp. 43-56, 2020.

[3] S. Ali, Z. Zheng, M. Aillerie, J.-P. Sawicki, M.-C. Pera, and D. Hissel, "A review of DC Microgrid energy management systems dedicated to residential applications," *Energies,* vol. 14, no. 14, p. 4308, 2021.

[4] G. Chen, F. L. Lewis, E. N. Feng, and Y. Song, "Distributed optimal active power control of multiple generation systems," *IEEE Transactions on Industrial Electronics,* vol. 62, no. 11, pp. 7079-7090, 2015.

[5] R. Khan *et al.*, "Energy sustainability–survey on technology and control of microgrid, smart grid and virtual power plant," *IEEE Access,* vol. 9, pp. 104663-104694, 2021.

[6] P. Venkata, V. Pandya, and A. Sant, "Data Mining Model Based Differential Microgrid Fault Classification Using SVM Considering Voltage and Current Distortions," *Journal of Operation and Automation in Power Engineering,* vol. 11, no. 3, pp. 162-172, 2023.

[7] A. Fathi, Q. Shafiee, and H. Bevrani, "Robust frequency control of microgrids using an extended virtual synchronous generator," *IEEE Transactions on Power Systems,* vol. 33, no. 6, pp. 6289-6297, 2018.

[8] K. Y. Yap, C. R. Sarimuthu, and J. M.-Y. Lim, "Virtual inertia-based inverters for mitigating frequency instability in grid-connected renewable energy system: A review," *Applied Sciences,* vol. 9, no. 24, p. 5300, 2019.

[9] K. C. Divya and J. Østergaard, "Battery energy storage technology for power systems—An overview," *Electric power systems research,* vol. 79, no. 4, pp. 511-520, 2009.

[10] X. Tan, Q. Li, and H. Wang, "Advances and trends of energy storage technology in microgrid," *International Journal of Electrical Power & Energy Systems,* vol. 44, no. 1, pp. 179-191, 2013.

[11] T. Madiba, R. Bansal, N. Mbungu, M. Bettayeb, R. Naidoo, and M. Siti, "Under-frequency load shedding of microgrid systems: a review," *International Journal of Modelling and Simulation,* vol. 42, no. 4, pp. 653-679, 2022.

[12] J. Singh, S. Prakash Singh, K. Shanker Verma, A. Iqbal, and B. Kumar, "Recent control techniques and management of AC microgrids: A critical review on issues, strategies, and future trends," *International Transactions on Electrical Energy Systems,* vol. 31, no. 11, p. e13035, 2021.

[13] S. K. Jha, D. Kumar, and M. Lehtonen, "Modified VI droop-based adaptive vector control scheme for demand side management in a stand-alone microgrid," *International Journal of Electrical Power & Energy Systems,* vol. 130, p. 106950, 2021.

[14] M. Azimian, V. Amir, R. Habibifar, and H. Golmohamadi, "Probabilistic optimization of networked multi-carrier microgrids to enhance resilience leveraging demand response programs," *Sustainability,* vol. 13, no. 11, p. 5792, 2021.

[15] Y. Liu, H. Wang, and C. Hou, "Sliding-mode control design for nonlinear systems using probability density function shaping," *IEEE transactions on neural networks and learning systems,* vol. 25, no. 2, pp. 332-343, 2013.

[16] I. Kumarswamy, T. K. Sandipamu, and V. Prasanth, "Analysis of islanding detection in distributed generation using fuzzy logic technique," in *2013 7th Asia Modelling Symposium*, 2013: IEEE, pp. 3-7.

[17] M. N. Acosta *et al.*, "Improvement of the frequency response indicators by optimal UFLS scheme settings," in *2020 IEEE 29th International Symposium on Industrial Electronics (ISIE)*, 2020: IEEE, pp. 1250-1255.

[18] L. Sigrist, L. Rouco, and F. M. Echavarren, "A review of the state of the art of UFLS schemes for isolated power systems," *International Journal of Electrical Power & Energy Systems,* vol. 99, pp. 525-539, 2018.

[19] P. Lakra and M. Kirar, "Load shedding techniques for systems with cogeneration: A review," *Electrical and Electronics Engineering: An International Journal (ELELIJ) Vol,* vol. 4, 2015.

[20] M. Zadehbagheri, M. Kiani, and S. Khandan, "Designing a Robust SMC for Voltage and Power Control in Islanded Micro-grid and Simultaneous Use of Load Shedding Method," *Journal of Operation and Automation in Power Engineering,* vol. 13, no. 1, pp. 74-87, 2025.

[21] H. Seyedi and M. Sanaye-Pasand, "New centralised adaptive load-shedding algorithms to mitigate power system blackouts," *IET generation, transmission & distribution,* vol. 3, no. 1, pp. 99-114, 2009.

[22] U. Rudez and R. Mihalic, "A novel approach to underfrequency load shedding," *Electric Power Systems Research,* vol. 81, no. 2, pp. 636-643, 2011.

[23] D. Bai, J. He, X. Yang, B. Kirby, D. Writer, and L. Liu, "Under frequency load shedding scheme based on information sharing technology," in *22nd International Conference and Exhibition on Electricity Distribution (CIRED 2013)*, 2013: IET, p. 0468.

[24] K. Mollah and N. C. Nair, "Coordinated strategy for under-voltage and under-frequency load shedding," in *2010 20th Australasian Universities Power Engineering Conference*, 2010: IEEE, pp. 1-6.

[25] U. Rudez and R. Mihalic, "WAMS-based underfrequency load shedding with short-term frequency prediction," *IEEE Transactions on Power Delivery,* vol. 31, no. 4, pp. 1912-1920, 2015.

[26] B. Hoseinzadeh and C. L. Bak, "Centralized coordination of emergency control and protection system using online outage

sensitivity index," *Electric Power Systems Research,* vol. 163, pp. 413-422, 2018.

[27] T. Shekari, A. Gholami, F. Aminifar, and M. Sanaye-Pasand, "An adaptive wide-area load shedding scheme incorporating power system real-time limitations," *IEEE Systems Journal,* vol. 12, no. 1, pp. 759-767, 2016.

[28] B. Hoseinzadeh, F. M. F. Da Silva, and C. L. Bak, "Adaptive tuning of frequency thresholds using voltage drop data in decentralized load shedding," *IEEE Transactions on Power Systems,* vol. 30, no. 4, pp. 2055-2062, 2014.

[29] B. Hoseinzadeh, F. F. da Silva, and C. L. Bak, "Decentralized coordination of load shedding and plant protection considering high share of RESs," *IEEE Transactions on Power Systems,* vol. 31, no. 5, pp. 3607-3615, 2015.

[30] P. Mahat, Z. Chen, and B. Bak-Jensen, "Underfrequency load shedding for an islanded distribution system with distributed generators," *IEEE Transactions on Power Delivery,* vol. 25, no. 2, pp. 911-918, 2009.

[31] W. Gu *et al.*, "Adaptive decentralized under-frequency load shedding for islanded smart distribution networks," *IEEE Transactions on Sustainable Energy,* vol. 5, no. 3, pp. 886-895, 2014.

[32] W. Liu *et al.*, "Improved average consensus algorithm based distributed cost optimization for loading shedding of autonomous microgrids," *International Journal of Electrical Power & Energy Systems,* vol. 73, pp. 89-96, 2015.

[33] M. Marzband, M. M. Moghaddam, M. F. Akorede, and G. Khomeyrani, "Adaptive load shedding scheme for frequency stability enhancement in microgrids," *Electric Power Systems Research,* vol. 140, pp. 78-86, 2016.

[34] M. Karimi, P. Wall, H. Mokhlis, and V. Terzija, "A new centralized adaptive underfrequency load shedding controller for microgrids based on a distribution state estimator," *IEEE Transactions on Power Delivery,* vol. 32, no. 1, pp. 370-380, 2016.

[35] S. Chandak, P. Bhowmik, and P. K. Rout, "Load shedding strategy coordinated with storage device and D-STATCOM to enhance the microgrid stability," *Protection and Control of Modern Power Systems,* vol. 4, no. 3, pp. 1-19, 2019.

[36] M. Rezaee, S. Mortazavi, and A. Saffarian, "Combination UFLS and UVLS Aim to Restore Frequency and Voltage Stability Simultaneously," in *2025 Fifth National and the First International Conference on Applied Research in Electrical Engineering (AREE)*, 2025: IEEE, pp. 1-7.

[37] N. Pogaku, M. Prodanovic, and T. C. Green, "Modeling, analysis and testing of autonomous operation of an inverter-based microgrid," *IEEE Transactions on Power Electronics,* vol. 22, no. 2, pp. 613-625, 2007.

[38] S. Tabatabaee, H. R. Karshenas, A. Bakhshai, and P. Jain, "Investigation of droop characteristics and X/R ratio on small-signal stability of autonomous microgrid," in *2011 2nd Power Electronics, Drive Systems and Technologies Conference*, 2011: IEEE, pp. 223-228.

[39] A. Mehrizi-Sani and R. Iravani, "Potential-function based control of a microgrid in islanded and grid-connected modes," *IEEE Transactions on Power Systems,* vol. 25, no. 4, pp. 1883-1891, 2010.

[40] J. M. Guerrero, J. C. Vasquez, J. Matas, L. G. De Vicuña, and M. Castilla, "Hierarchical control of droop-controlled AC and DC microgrids—A general approach toward standardization," *IEEE Transactions on Industrial Electronics,* vol. 58, no. 1, pp. 158-172, 2010.

[41] M. C. Chandorkar, D. M. Divan, and R. Adapa, "Control of parallel connected inverters in standalone AC supply systems," *IEEE transactions on industry applications,* vol. 29, no. 1, pp. 136-143, 2002.

[42] P. M. Anderson and M. Mirheydar, "An adaptive method for setting underfrequency load shedding relays," *IEEE Transactions on Power Systems,* vol. 7, no. 2, pp. 647-655, 1992.

[43] Y. Bo, X. Da, C. Chen, G. Fang, and L. Xiaobo, "Current status of low frequency load shedding in power system and its application," *East China Electric Power,* vol. 9, pp. 14-18, 2002.

[44] V. V. Terzija, "Adaptive underfrequency load shedding based on the magnitude of the disturbance estimation," *IEEE Transactions on Power Systems,* vol. 21, no. 3, pp. 1260-1266, 2006.

[45] S.-J. Huang and C.-C. Huang, "An adaptive load shedding method with time-based design for isolated power systems," *International Journal of Electrical Power & Energy Systems,* vol. 22, no. 1, pp. 51-58, 2000.

[46] C. Li *et al.*, "Continuous under-frequency load shedding scheme for power system adaptive frequency control," *IEEE Transactions on Power Systems,* vol. 35, no. 2, pp. 950-961, 2019.

[47] E. Dehghanpour, H. K. Karegar, and R. Kheirollahi, "Under frequency load shedding in inverter-based microgrids by using droop characteristic," *IEEE Transactions on Power Delivery,* vol. 36, no. 2, pp. 1097-1106, 2020.

[48] S. M. S. Kalajahi, H. Seyedi, and K. Zare, "Under-frequency load shedding in isolated multi-microgrids," *Sustainable Energy, Grids and Networks,* vol. 27, p. 100494, 2021.

[49] C. Luo, H. G. Far, H. Banakar, P.-K. Keung, and B.-T. Ooi, "Estimation of wind penetration as limited by frequency deviation," in *2006 IEEE Power Engineering Society General Meeting*, 2006: IEEE, p. 8 pp.

[50] A. Ketabi and M. H. Fini, "An underfrequency load shedding scheme for islanded microgrids," *International Journal of Electrical Power & Energy Systems,* vol. 62, pp. 599-607, 2014.

[51] N. T. Mbungu, R. Naidoo, R. C. Bansal, and M. Bipath, "Optimisation of grid connected hybrid photovoltaic–wind–battery system using model predictive control design," *IET Renewable Power Generation,* vol. 11, no. 14, pp. 1760-1768, 2017.

[52] M. Khonji, C.-K. Chau, and K. Elbassioni, "Optimal power flow with inelastic demands for demand response in radial distribution networks," *IEEE Transactions on Control of Network Systems,* vol. 5, no. 1, pp. 513-524, 2016.

[53] M. A. Allam, A. A. Hamad, M. Kazerani, and E. F. El-Saadany, "A novel dynamic power routing scheme to maximize loadability of islanded hybrid AC/DC microgrids under unbalanced AC loading," *IEEE Transactions on Smart Grid,* vol. 9, no. 6, pp. 5798-5809, 2017.

[54] L. Gidwani, H. Tiwari, and R. Bansal, "Improving power quality of wind energy conversion system with unconventional power electronic interface," *International Journal of Electrical Power & Energy Systems,* vol. 44, no. 1, pp. 445-453, 2013.

[55] M. Talaat, A. Hatata, A. S. Alsayyari, and A. Alblawi, "A smart load management system based on the grasshopper optimization algorithm using the under-frequency load shedding approach," *Energy,* vol. 190, p. 116423, 2020.

[56] Y. Levron, J. M. Guerrero, and Y. Beck, "Optimal power flow in microgrids with energy storage," *IEEE Transactions on Power Systems,* vol. 28, no. 3, pp. 3226-3234, 2013.

[57] Y. Dong, X. Xie, K. Wang, B. Zhou, and Q. Jiang, "An emergency-demand-response based under speed load shedding scheme to improve short-term voltage stability," *IEEE Transactions on Power Systems,* vol. 32, no. 5, pp. 3726-3735, 2017.

[58] S. S. Reddy, "Multi-objective based congestion management using generation rescheduling and load shedding," *IEEE Transactions on Power Systems,* vol. 32, no. 2, pp. 852-863, 2016.

[59] Q. Xu, B. Yang, Q. Han, Y. Yuan, C. Chen, and X. Guan, "Optimal power management for failure mode of MVDC microgrids in all-electric ships," *IEEE Transactions on Power Systems,* vol. 34, no. 2, pp. 1054-1067, 2018.